Two-Level Islanding Detection Method for Grid-Connected Photovoltaic System-Based Microgrid with Small Non-Detection Zone

Bakhshi-Jafarabadi, Reza; de Jesus Chavez, Jose; Sadeh, Javad ; Popov, M.

Important note
To cite this publication, please use the final published version (if applicable).
Please check the document version above.

Two-Level Islanding Detection Method for Grid-Connected Photovoltaic System-Based Microgrid With Small Non-Detection Zone

Reza Bakhshi-Jafarabadi[ID], Javad Sadeh[ID], Jose de Jesus Chavez[ID], *Member, IEEE*, and Marjan Popov[ID], *Senior Member, IEEE*

Abstract—This article proposes a fast and reliable two-level islanding detection method (IDM) for grid-connected photovoltaic system (GCPVS)-based microgrid. In the first level of the proposed IDM, the magnitude of the rate of change of output voltage (ROCOV) is computed. If this variable exceeds a predefined threshold, a disturbance is injected into the duty cycle of DC/DC converter after a given time delay to deviate the system operating point away of its maximum power point (MPP) condition. This leads to a substantial active power output and voltage reduction in an islanded mode. Therefore, the ROCOV and the rate of change of active power output (ROCOP) indices, measured in the second stage, pose great negative sets at the same time in islanding states. However, the variation of at least one of these variables is near-zero in non-islanding switching events. The assessment of the presented algorithm has been conducted under extensive islanding and non-islanding scenarios for a case study system with two PV power plants using hardware-in-the-loop (HiL) simulation tests. The provided results remark precise islanding classification with an eminently small non-detection zone (NDZ) within 510 ms. The presented IDM has the advantages of self-standing thresholds determination, no improper effect on the output power quality, and simple and inexpensive structure. Moreover, the fast MPP restoration of the proposed scheme after islanding identification boosts the chance of seamless reconnection and DG autonomous operation in microgrid.

Index Terms—Grid-connected photovoltaic system (GCPVS), islanding detection method (IDM), maximum power point (MPP), microgrid, non-detection zone (NDZ), rate of change of active power output (ROCOP), rate of change of output voltage (ROCOV).

I. INTRODUCTION

GRID-CONNECTED photovoltaic system (GCPVS) has been developed in the distribution network at steady-state pace over the past decade. In this regard, the global installed capacity of this technology recorded at 98.9 and 99.8 GW in 2017 and 2018, respectively [1].

Just as other distributed generators (DGs), the connection of GCPVS to the distribution network poses a few challenges such as islanding. Islanding refers to a condition in which the DG supplies solely a portion of the network when the utility is disconnected for the time being. This undesirable state should be detected timely to ensure power quality requirements, and safety of repair crew and sensitive equipment [2]. In this perspective, IEEE Standard 1547-2008 and UL 1741 impose a maximum of 2 seconds for ceasing energizing DG after island formation [3], [4]. Islanding detection is mandatory for microgrid operation to restore DG's generation at its highest possible level for voltage and frequency control purpose in standalone mode. A fast islanding classification and subsequent seamless reconnection is thereby required to accomplish this goal [5].

Various islanding detection methods (IDMs), generally categorized into local and communication-based (remote) techniques, have been reported [6]–[28]. Remote groups rely on a communication channel between upstream substation and DGs. By this means, islanding is identified when the broadcast signal is not detected by the signal receiver installed at the DG end [6], [7]. These reliable and fast schemes can be applied to both synchronous- and inverter-based DGs. The high burden cost is known as the main limitation, however.

In local techniques, including passive, active, and hybrid, a parameter of the point of common coupling (PCC) has been monitored continuously. Islanding is recognized in passive IDMs when a local yardstick deviates its pre-defined tolerable range. A few examples of the recently passive techniques can be found in [8]–[11]. Although these methods are realized smoothly and cost-effectively, they suffer from a large non-detection zone (NDZ), i.e., the situations with closely matched power generation and consumption that islanding remains undetected. The threshold selection is another challenge, which should be fulfilled as a compromise between minimum NDZ and nuisance tripping. Several mathematical tools have been newly introduced to extract a feature in the frequency-domain [12]–[14] or employ a pattern recognition algorithm [15]–[18] for islanding classification. These computational-based IDMs present smaller NDZ, the settings,

however, are highly depended on the case study system. In order to alleviate the NDZ, active IDMs that exploit an intentional disturbance to facilitate the deviation of local features in islanded mode, have been presented [19]–[25]. Although the injected disturbance enhances the NDZ and detection time, it deteriorates the power quality of the distribution network. Finally, hybrid strategies consisting in two local IDMs have been established to improve the NDZ and power quality degradation of passive and active methods [26]–[28]. The disturbance of the active IDM is stimulated whilst the suspicious islanding state has been detected by passive IDM. The power quality has not been thereby affected in normal operating conditions. Nevertheless, the complexity and costs are still known as the two main demerits of hybrid IDMs.

This article deals with a new two-level methodology for detecting islanding operation of GCPVSs. PV units work continuously at maximum power point (MPP) condition in a given meteorological state. This aim is achieved through an MPP tracking (MPPT) algorithm in the DC/DC converter of voltage source inverter (VSI). In the first stage of the proposed algorithm, the magnitude of the rate of change of PCC voltage (ROCOV) is measured and when it surpasses a threshold, a disturbance is triggered in the MPPT algorithm. This disturbance leads to a sharp active power output drop and as a result, a PCC voltage fall in islanding events. On the contrary, its influence on the output voltage is negligible during the DG parallel operation with the grid.

Some non-islanding incidents such as motor starting and capacitor bank disconnection can lead to a similar voltage variation, i.e., great negative ROCOV. Accordingly, a further condition including a high drop of the rate of change of active power output (ROCOP) has been established to avoid misclassification in such events. By this means, ROCOP and ROCOV do not pass the thresholds at the same time in non-islanding switching transients. Therefore, the simultaneous occurrence of the high negative levels for ROCOP and ROCOV in the second stage is the yardstick of the proposed algorithm.

In addition to an effective islanding detection with negligible NDZ, the main advantages of the presented IDM can be summarized as follows:
- Fast islanding classification in less than 510 ms.
- Applicable to microgrid for DG autonomous operation purpose regarding the fast MPP restoration.
- Straightforward and cost-competitive structure.
- Thresholds self-standing determination irrespective of the DG and grid characteristics.
- Implementable in other renewable resources with MPPT, e.g., wind farms, with a minimum effort.

The rest of the paper is organized as follows; Section II elaborates the proposed strategy as well as the thresholds selection criteria. In Section III, the test system containing two PV power plants equipped with two multi-function digital relays is introduced. The effectiveness of the proposed IDM has been then investigated in Section IV under extensive case studies through real-time hardware-in-the-loop (HiL) simulations. A comparative assessment of the proposed technique with a few existing IDMs is conducted in Section V
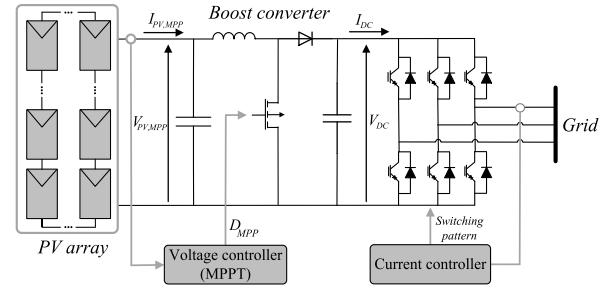

Fig. 1. Voltage and current control loops in VSI.
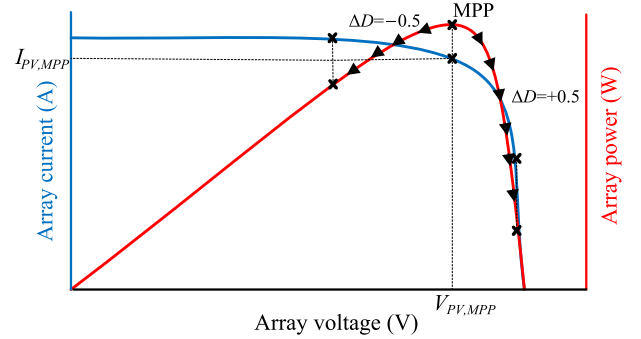
Fig. 2. MPPT and proposed IDM realization.

to highlight its overall outstanding performance. Concluding remarks are finally presented in Section VI.

II. DESCRIPTION OF THE PROPOSED METHODOLOGY

A. Two-Level Islanding Detection Algorithm

In GCPVSs, VSI consists of two independent control loops as depicted in Fig. 1. Current controller in the DC/AC converter transforms DC power to AC one, balances the input and output powers, and synchronizes output current to the grid voltage. The voltage control loop in the DC/DC converter is responsible for MPPT and DC voltage regulation [29]. MPPT has been accomplished through determining the duty cycle of DC/DC converter, e.g., boost converter in Fig. 1. The duty cycle has been set in a way that the PV array operating point settles at MPP in any solar insolation level (Fig. 2). In MPP mode, the relation of input and output voltages and currents of the DC/DC converter, e.g., boost converter, can be given by [30]:

$$\begin{cases} V_{DC} = \frac{V_{PV,MPP}}{1-D_{MPP}} \\ I_{DC} = I_{PV,MPP} \times (1 - D_{MPP}) \end{cases} \quad (1)$$

where, $V_{PV,MPP}$ and $I_{PV,MPP}$ are MPP voltage and current of the PV array. The DC link voltage and current are also denoted by V_{DC} and I_{DC}. In addition, the duty cycle corresponding to MPP is represented by D_{MPP}.

The first level of the proposed algorithm includes a measurement of the ROCOV magnitude at PCC with the system fundamental frequency (f_{sys}), i.e., $ROCOV_1$. The absolute voltage change has been used in $ROCOV_1$ calculation since PCC voltage can be raised or lowered after islanding. When this

Fig. 3. Flowchart of the proposed IDM.

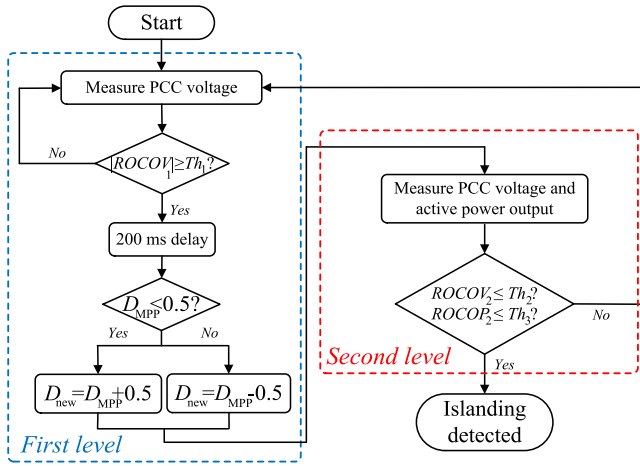Fig. 4. NDZ of the proposed IDM under various Th_1 settings.

parameter in any phase exceeds a threshold (Th_1), a disturbance is triggered in the duty cycle as follows:

$$\begin{cases} D_{new} = D_{MPP} - 0.5, & D_{MPP} \geq 0.5 \\ D_{new} = D_{MPP} + 0.5, & D_{MPP} < 0.5 \end{cases} \quad (2)$$

where, D_{new} is the new duty cycle after disturbance activation. This short-duration disturbance is switched OFF for a given time interval to restore MPP, e.g., 1.8 s. It is also inserted with an intentional 0.2 s time delay to avoid nuisance tripping during non-islanding events. Moreover, D_{new} has been defined as in (2) to achieve the most possible shift from MPP.

As shown in Fig. 2, the injected disturbance leads to a great active power output drop for both manners. In islanding mode, the post-islanding output voltage (V_{po}) can be defined by:

$$P_{DG} = \frac{V_{po}^2}{R} \quad (3)$$

where, P_{DG} represents for DG active power output and R is the resistive part of the parallel RLC local load model, defined in IEEE Standard 929-2000 [31]. According to (3), the output voltage has been dropped sharply in islanding states regarding the active power output reduction. It is, however, governed strictly by the power system in grid-tied mode and its variation is near-zero. Consequently, the measured ROCOV in the second stage ($ROCOV_2$) is shifted to the negative direction in islanding event.

Since a same variation of $ROCOV_2$ can be observed in a few non-islanding scenarios such as motor starting, capacitor disconnection, and abrupt load raise, a further condition has been established. $ROCOP_2$ is also greatly negative during the disturbance activation time frame regarding the above-mentioned explanation. Therefore, the simultaneous occurrence of great negative values for $ROCOV_2$ and $ROCOP_2$, i.e., lower than the predefined thresholds (Th_2 and Th_3), is the final yardstick of the proposed methodology.

In the presented IDM, since the duty cycle is re-established to D_{MPP} after a short transient, the DG transition from grid-tied to the autonomous mode in microgrid is facilitated. Moreover, it is readily observed from the method's flowchart in Fig. 3 that its integration to the existing VSIs is straightforward and cost-effective.
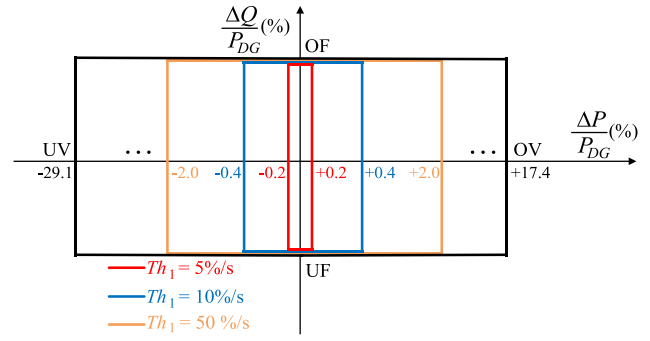
B. Selection Criteria of Threshold Settings

There are three settings in the proposed two-level IDM; the ROCOV threshold (Th_1) of the first stage which triggers the disturbance for MPP lost purpose; ROCOV and ROCOP thresholds (Th_2 and Th_3) of the second level which categorizes islanding and non-islanding incidents. The selection criteria of these variables are presented as follows.

1) ROCOV Threshold in First Level: The proposed disturbance is stimulated when $ROCOV_1$ exceeds Th_1. Hence, smaller NDZ can be achieved under lower Th_1 sets. On the other hand, the system operating point is deviated from MPP after disturbance injection, diminishing the active power output and efficiency. Nevertheless, the effect of imposed disturbance on efficiency is hardly appreciable since the MPP lost duration is very short. Therefore, the focus of this part is on Th_1 determination in the term of NDZ.

In this regard, (4) is initially used to define the PCC voltage after grid isolation regarding the relative active power mismatch ($\Delta P / P_{DG}$) between DG generation and load demand:

$$\frac{\Delta V_{PCC}}{V_{pr}} = \sqrt{\frac{1}{1 - \frac{\Delta P}{P_{DG}}} - 1} \quad (4)$$

where, V_{pr} and ΔV_{PCC} are pre-islanding PCC voltage and its variation after islanding phenomena, i.e., $V_{po} = V_{pr} + \Delta V_{PCC}$. This shift is exploited to define $ROCOV_1$ regarding the measurement time window ($1/f_{sys}$), e.g., 20 ms in the current article:

$$ROCOV_1 = \frac{|\Delta V_{PCC}|}{V_{pr}} \times f_{sys} \quad (5)$$

Equations (4) and (5) can be employed to compute NDZ with respect to the relative active power mismatch. In order to achieve a given NDZ, Th_1 should be smaller than the measured $ROCOV_1$. For instance, the disturbance is stimulated in the case of relative active power mismatch outside the [−0.4%, 0.4%] range for $Th_1 = 10\%/s$ under $V_{pr} = 100\%$.

Fig. 4 indicates the method's NDZ for a few Th_1 settings in where OV/UV and OF/UF stand for over/under voltage and over/under frequency relays' sets. It is clearly seen that the proposed IDM provides a very small NDZ, e.g., [−0.4%, 0.4%] under $Th_1 = 10\%/s$ which is around 98% lower than the commercial voltage relay's one with [−29.1%, 17.4%] NDZ.

2) Settings in Second Level: The second stage discriminates islanding and non-islanding events through comparing $ROCOV_2$ and $ROCOP_2$ with 200 ms measurement time window to Th_2 and Th_3. These indices have been pushed simultaneously to the negative direction in islanding conditions while the variation of at least one of them is negligible during other incidents. Hence, the settings Th_2 and Th_3 should be defined in a way that $ROCOV_2$ and $ROCOP_2$ go beyond them in islanding circumstances.

After disturbance injection, the GCPVS jumps to the new operating point; and PV array's voltage and current can be expressed as:

$$\begin{cases} V_{DC,new} = \frac{V_{PV,new}}{(1-D_{new})} \\ I_{DC,new} = I_{PV,new} \times (1 - D_{new}) \end{cases} \quad (6)$$

where, "*new*" implies the new operating point. The active power shift due to the employed disturbance can be quantified through the new array's voltage and current as:

$$P_{PV,new} = V_{PV,new} \times I_{PV,new} \quad (7)$$

Afterward, the ratio of the new active power to the MPP one ($P_{PV,MPP}$) can be given by:

$$\begin{cases} \frac{P_{PV,new}}{P_{PV,MPP}} = \frac{V_{PV,new}}{V_{PV,MPP}} \times \frac{I_{PV,new}}{I_{PV,MPP}} \simeq \frac{I_{PV,new}}{I_{PV,MPP}}, \\ \qquad\qquad\qquad\qquad\qquad V_{PV,new} \geq V_{PV,MPP} \\ \frac{P_{PV,new}}{P_{PV,MPP}} = \frac{V_{PV,new}}{V_{PV,MPP}} \times \frac{I_{PV,new}}{I_{PV,MPP}} \simeq \frac{V_{PV,new}}{V_{PV,MPP}}, \\ \qquad\qquad\qquad\qquad\qquad V_{PV,new} < V_{PV,MPP} \end{cases} \quad (8)$$

According to Fig. 2, the first expression in (8) is approximated by neglecting the variation of PV voltage in the right-hand side of MPP; the PV current variation is also small in comparison to its voltage change in the left-hand side of MPP (second term). These expressions can be more simplified as in (9) by combining (1) and (8) and neglecting $I_{DC,new}/I_{DC,MPP}$ and $V_{DC,new}/V_{DC,MPP}$ against the final terms, e.g., for boost converter:

$$\begin{cases} \frac{P_{PV,new}}{P_{PV,MPP}} = \frac{1-D_{MPP}}{1-D_{new}}, & V_{PV,new} \geq V_{PV,MPP} \\ \frac{P_{PV,new}}{P_{PV,MPP}} = \frac{1-D_{new}}{1-D_{MPP}}, & V_{PV,new} < V_{PV,MPP} \end{cases} \quad (9)$$

The relative active power disturbance can be finally deduced by defining active power change caused by the applied disturbance as $\Delta P_{DIS} = P_{PV,new} - P_{PV,MPP}$ and referring to (2):

$$\begin{cases} \frac{\Delta P_{DIS}}{P_{PV,MPP}} = \frac{-0.5}{1.5-D_{MPP}}, & V_{PV,new} \geq V_{PV,MPP} \\ \frac{\Delta P_{DIS}}{P_{PV,MPP}} = \frac{-0.5}{1-D_{MPP}}, & V_{PV,new} < V_{PV,MPP} \end{cases} \quad (10)$$

It is worth mentioning that the same criteria can be employed to the other DC/DC converter types; for instance, the relative active power disturbance of the buck converter is $-0.5/D_{MPP}$ for $V_{PV,new} \geq V_{PV,MPP}$ and $-0.5/(D_{MPP} + 0.5)$ for $V_{PV,new} < V_{PV,MPP}$. Thereafter, (4) is manipulated to figure out the relative voltage change ($\Delta V'_{PCC}/V_{po}$) caused by the relative active power disturbance:

$$\frac{\Delta V'_{PCC}}{V_{po}} = \sqrt{\frac{1}{1 - \frac{\Delta P_{DIS}}{P_{DG}}} - 1} \quad (11)$$
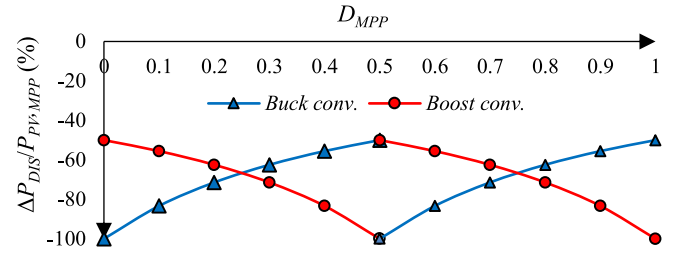

Fig. 5. The effect of proposed disturbance on the active power output.
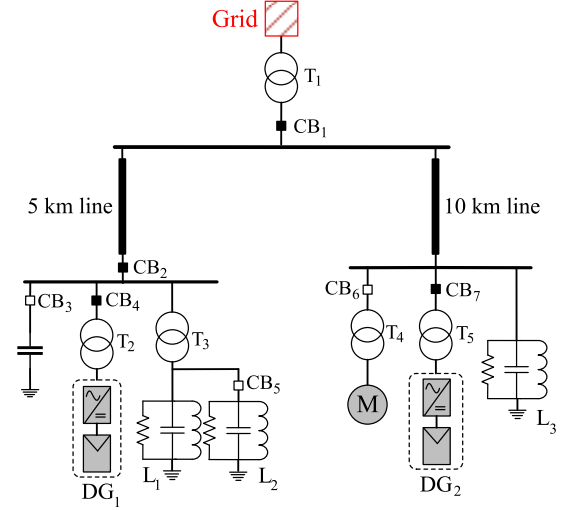
Fig. 6. The schematic of the test system under study.

This equation shows the output voltage shift after disturbance injection by neglecting the VSI losses, i.e., $P_{DG} = P_{PV,MPP}$. $ROCOV_2$ and $ROCOP_2$ can be defined eventually regarding the measurement time frame of the second level that is 200 ms (ten cycles):

$$\begin{cases} ROCOV_2 = \frac{\Delta V'_{PCC}}{V_{po}} \times 0.1 \times f_{sys} \\ ROCOP_2 = \frac{\Delta P_{DIS}}{P_{DG}} \times 0.1 \times f_{sys} \end{cases} \quad (12)$$

The variation of relative active power disturbance for buck and boost converters under various D_{MPP} is shown in Fig. 5. As it can be seen, its minimum drop is -50%; the respective $ROCOV_2$ and $ROCOP_2$ are $-80.74\%/s$ and $-250\%/s$ under $f_{sys} = 50$ Hz, $P_{DG} = 100\%$, and $V_{po} = 88\%$ as the worst post-islanding scenario according to (11).

In the presented analysis, the threshold settings have been hence assigned as $Th_1 = 10\%/s$, $Th_2 = -30\%/s$, and $Th_3 = -100\%s/$. This selection ensures proposed disturbance activation under relative active power mismatches outside of the narrow range $[-0.4\%, 0.4\%]$ and precise classification of islanding and non-islanding events. Furthermore, these settings are determined as self-standing disregarding the system and DG characteristics.

III. CASE STUDY SYSTEM MODEL

The proposed two-level IDM has been evaluated under numerous case studies for a radial distribution network depicted in Fig. 6 and detailed in Table I. Two parallel feeders, each containing a 1 MW PV power plant and local load,

TABLE I
SETTINGS OF THE CASE STUDY SYSTEM

Equipment	Description
Utility	400 kV, 1000 MVA, 50 Hz
Line	Z^1=0.034+j0.312 Ω/km, Z^0=0.232+0.91 Ω/km
Transformer*	T_1: 2.5 MVA, 400/13.2 kV; T_2, T_5: 1.2 MVA, 13.2/0.4 kV; T_3: 2.5 MVA, 13.2/0.4 kV; T_4: 2.5 MVA, 13.2/0.4 kV
GCPVS	DG_1: 1 MW at STC (Q.PEAK-G4.1 300) V_{OC}=39.76 V, I_{SC}=9.77 A , V_{MPP}=32.41 V , I_{MPP}=9.26 A DG_2: 1 MW at STC (YL305P-35b) V_{OC}=46.3 V, I_{SC}=8.87 A , V_{MPP}=37.0 V , I_{MPP}=8.25 A
Asynchronous motor	1000–3000 HP, 0.4 kV, R_s=0.0425 p.u., L_s=0.087 p.u., R_r=0.05 p.u., L_r=0.0658 p.u., L_m=2.9745 p.u.

* All connected in ΔY11.
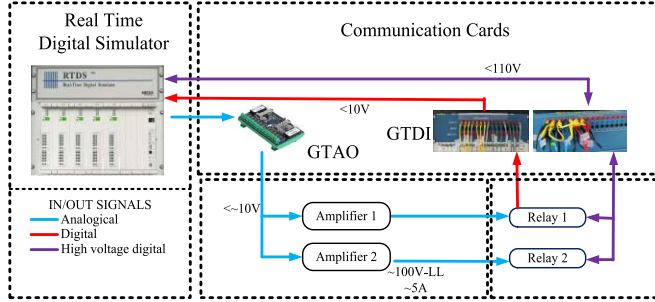
Fig. 7.   Implementation of the HiL tests in RTDS environment.

Fig. 8.   Results of case 3 with 1% active and reactive powers surplus.

have been connected to a 400 kV network. The parallel RLC local loads which represent the household (L_1 and L_2) and commercial demands (L_3), are designed to consume nominal output power of DGs at standard test condition (STC), i.e., the situation with 1000 W/m^2 received insolation and 25°C cell temperature.

The first GCPVS exploits a boost converter with perturb and observe MPPT algorithm while the second one is equipped with a buck converter with incremental conductance algorithm [30]. This selection provides the chance of islanding assessment under different converter topologies and MPPT algorithms.

The studied system is fully modeled in a real-time environment and simulated by four real-time digital simulator (RTDS) PB5 cards. In HiL, a pair of commercial multi-function relays with settings matched with IEEE Standard 1547-2008 [3] are integrated at the DGs' ends (CB_4 and CB_7 in Fig. 6). In order to interface the electrical signals from the PCCs to the relays, two amplifiers and one gigabit transceiver analogue card (GTAO) are used. The front digital input/output panel is also employed to interface the binary signals from/to the relays namely trips, reclosing, and circuit breakers status as displayed in Fig. 7. The islanding detection signal as the output of the proposed methodology is sent to the relays for DG(s) disconnection in conventional power system or settings change purpose for standalone operation in microgrid.

IV. EVALUATION OF THE PROPOSED METHODOLOGY

In this section, the authenticity of the suggested IDM has been investigated under extensive islanding and non-islanding scenarios. These events have been incepted at $t = 2$ s through

opening or closing circuit breakers (CBs) in Fig. 6. The islanding case studies at the presence of a 1 MW GCPVS have been realized by opening CB_2 while CB_1 is opened to simulate islanding scenarios at the presence of multiple DGs. These cases include various active/reactive power mismatches under STC and other operating modes, different load quality factors, static loads, and multiple DGs. The real-time HiL simulations for all cases have been presented and thoroughly analyzed.

A. Active/Reactive Power Mismatch (Cases 1–9)

The amount of relative active power mismatch is a key variable in the analysis of the voltage-based IDMs. According to (4), the post-islanding PCC voltage does not leave the voltage standard limits when relative active power mismatch lies inside the range [−29.1%, 17.4%] (Fig. 4). Moreover, islanding standards emphasize on conducting the tests under different relative active and reactive power mismatches up to ±5% [3], [4]. The initial study has been accordingly developed for a set of active and reactive power imbalances (ΔP and ΔQ in Table II) inside the voltage relays' NDZ (cases 1–9). The results, including duty cycle, DG active power, $ROCOV_1$, $ROCOV_2$, and $ROCOP_2$ for case 3 are displayed in Fig. 8. The measured $ROCOV_1$, $ROCOV_2$, $ROCOP_2$, and the detection time of the other case studies are also presented in Table II. In this table, $ROCOV_1$ indicates the first recorded ROCOV larger than Th_1 except in case 1 which represents the greatest ROCOV.

Fig. 8 shows that $ROCOV_1$ surpasses Th_1 after 40 ms (two cycles) of islanding onset. The proposed disturbance is

TABLE II
RESULTS FOR DIFFERENT ISLANDING SCENARIOS

Test no.	Test type	Load(s) demand	$\Delta P/P_{DG}$ (%)	$\Delta Q/P_{DG}$ (%)	$ROCOV_1$ (%/s)	$ROCOV_2$ (%/s)	$ROCOP_2$ (%/s)	**Detection time (ms)**
1	Active and reactive power mismatch at STC (Opening CB₂)	1 MW	−	−	0.30	−	−	−
2		0.99 MW, 0.01 Mvar	+1	-1	22.80	-271.97	-402.56	**413**
3		0.99 MW, -0.01 Mvar	+1	+1	16.31	-281.17	-411.28	**398**
4		1.01 MW, 0.01 Mvar	-1	-1	10.43	-261.09	-389.74	**437**
5		1.01 MW, -0.01 Mvar	-1	+1	11.58	-248.95	-393.64	**379**
6		0.95 MW, 0.05 Mvar	+5	-5	69.41	-292.41	-401.03	**424**
7		0.95 MW, -0.05 Mvar	+5	+5	16.45	-223.91	-374.60	**322**
8		1.05 MW, 0.05 Mvar	-5	-5	39.68	-264.89	-396.27	**437**
9		1.05 MW, -0.05 Mvar	-5	+5	34.79	-265.01	-401.96	**398**
10	Active and reactive power mismatch at 75% of STC (Opening CB₂)	0.7425 MW, 7.5 kvar	+1	-1	12.74	-258.13	-398.98	**349**
11		0.7425 MW, -7.5 kvar	+1	+1	13.53	-273.21	-327.09	**449**
12		0.7575 MW, 7.5 kvar	-1	-1	15.14	-258.92	-404.20	**366**
13		0.7575 MW, -7.5 kvar	-1	+1	15.29	-260.41	-304.19	**373**
14	Active and reactive power mismatch at 50% of STC (Opening CB₂)	0.495 MW, 5 kvar	+1	-1	25.32	-303.84	-381.54	**458**
15		0.495 MW, -5 kvar	+1	+1	11.80	-261.79	-281.27	**469**
16		0.505 MW, 5 kvar	-1	-1	18.65	-171.30	-346.04	**365**
17		0.505 MW, -5 kvar	-1	+1	13.69	-164.72	-346.40	**323**
18	Load quality factor at STC R_L=404.04 Ω L_L=1.2861/Q_f H C_L= 7.8782×Q_f µF (Opening CB₂)	0.99 MW (Q_f=0.5)	+1	−	18.83	-282.86	-411.68	**419**
19		0.99 MW (Q_f=1.0)	+1	−	13.07	-274.12	-394.59	**451**
20		0.99 MW (Q_f=1.5)	+1	−	17.34	-267.15	-399.60	**387**
21		0.99 MW (Q_f=2.0)	+1	−	15.60	-269.11	-296.08	**469**
22		0.99 MW (Q_f=2.5)	+1	−	12.37	-264.71	-402.21	**405**
23	Static load (Opening CB₂) P_L^0 =0.99 MW	p_Z=0.0, p_I=0.0, p_P=1.0	+1	−	10.10	-319.09	-303.02	**338**
24		p_Z=0.008, p_I=-0.023, p_P=1.015	+1	−	21.86	-338.29	-356.98	**379**
25		p_Z=0.43, p_I=0.69, p_P=-0.12	+1	−	27.43	-200.17	-241.98	**331**
26		p_Z=0.012, p_I=-0.032, p_P=1.02	+1	−	44.52	-426.63	-379.93	**424**
27		p_Z=1.0, p_I=0.0, p_P=0.0	+1	−	16.08	-302.40	-372.21	**392**
28	Multiple DGs connection (Opening CB₁)	2.02 MW, 0.02 Mvar	+1	-1	10.8/10.1	-229/-229	-384/-385	**475**
29		2.02 MW, -0.02 Mvar	+1	+1	12.1/12.0	-298/-308	-344/-458	**510**
30		1.98 MW, 0.02 Mvar	-1	-1	14.1/12.7	-299/-317	-313/-443	**470**
31		1.98 MW, -0.02 Mvar	-1	+1	11.8/10.2	-343/-343	-413/-501	**432**

consequently triggered after the intentional 200 ms, shifting the GCPVS operating point from MPP. This MPP deviation leads to a notable active power output and PCC voltage reduction. Therefore, $ROCOV_2$ and $ROCOP_2$ pass Th_2 and Th_3 and islanding is classified at $t = 2.398$ s time instance.

The provided data in Table II also highlight reliable performance of the current methodology in all cases except in the well-balanced island (case 1). In this state, the disturbance has not been stimulated due to the small $ROCOV_1$ and islanding remains undetected. Accordingly, the NDZ includes -0.4% to 0.4% range of $\Delta P/P_{DG}$ for $Th_1 = 10\%$/s in which the disturbance has not been actuated.

B. Non-STC Operational Mode (Cases 10–17)

GCPVSs are variable energy resources which operate in a wide range of insolation and temperature levels. The proposed IDM should exhibit secure performance for various penetration levels. In cases 10–17, islanding is yielded for P_{DG} set at 75% and 50% of the STC power. The load elements have been tuned in a way that power consumption would be close to the DG generation. The response of the two-level strategy to the islanding event in two non-STCs is illustrated in Fig. 9.

The results reveal clearly successful islanding classification as well as output voltage and active power restoration to post-islanding and MPP levels, respectively. Since the output voltage and active power settle at their steady-state sets after islanding detection, the DG transition process to operate in standalone mode is fully facilitated.
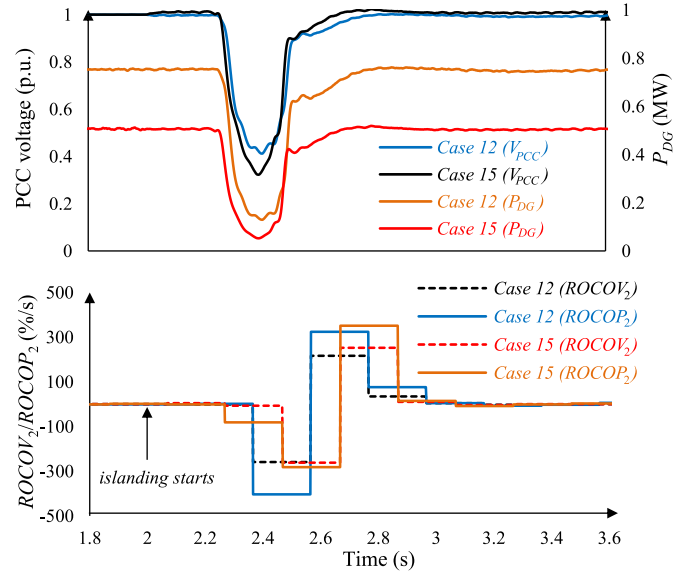
Fig. 9. Results of non-full rated output power.

C. Load Quality Factor (Cases 18–22)

This part explores the functionality of the presented algorithm under various load quality factors (Q_fs), another variable which can affect substantially the results. IEEE Standard 1547-2008 and UL 1741 recommend islanding assessment under Q_f lower than 2.5 and 1, respectively [3], [4]. The load parameters have been designed in cases 18–22 to present several Q_fs
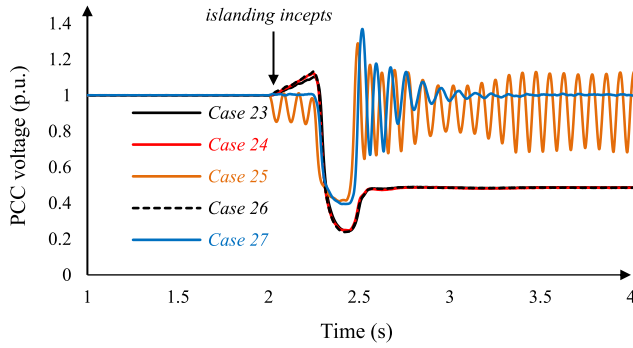
Fig. 10.   Static load influence on performance of the proposed approach.

TABLE III
CASE STUDIES AND OUTPUTS OF NON-ISLANDING STUDY

Test no.	Test type	Power change	$ROCOV_2/ROCOP_2$ (%/s)	
			During event	During IDM firing
32	Capacitor bank disconnection (Opening CB$_3$)	1 Mvar	-0.6/-1.3	-3.2/1.6
33		2 Mvar	-1.3/1.2	-0.5/-173.6
34		3 Mvar	-24.0/4.4	-4.4/-168.7
35		4 Mvar	-34.5/1.1	-1.0/-308.5
36		5 Mvar	-44.4/-1.0	-0.4/-371.2
37	Motor starting (Closing CB$_6$)	250 HP	-0.1/-0.1	0/1.6
38		500 HP	-0.3/0.2	-0.5/-0.3
39		1000 HP	-10.8/-9.1	1.8/-459.6
40		2000 HP	-17.3/-24.7	7.2/-503.8
41		3000 HP	-28.6/-9.1	9.4/-494.9
42	Abrupt load switch (Closing CB$_5$)	1 MW	-1.0/0.5	-1.0/-302.1
43		1 MW, 1 Mvar	-8.3/2.7	-1.1/-168.1
44		1 MW, -1 Mvar	-3.2/2.0	-6.6/-394.1

with around 50 Hz resonant frequency and small active power mismatch.

As it can be viewed in Table II, the $ROCOV_2$ and $ROCOP_2$ are timely and precisely drifted to the lower direction in all cases. Since the response of islanded area to the injected disturbance is almost the same in all scenarios disregarding the available power mismatches, the detection time lies within the 300–500 ms time frame which is much lower than the permissible time postulated in islanding standards [3], [4]. It is small enough for voltage and frequency stabilization in standalone operational mode of microgrid as well.

D. Static Load (Cases 23–27)

Most loads represent voltage- and frequency-based behavior in real test conditions. The performance of a two-level IDM under the connection of constant impedance, current, and power (ZIP) load is hence crucial. In cases 23–27, the load active power (P_L) is supposed to have the following characteristics with focus on voltage dependency:

$$P_L^1 = P_L^0 \times \left(p_Z \left(\frac{V_{PCC}^1}{V_{PCC}^0} \right)^2 + p_I \left(\frac{V_{PCC}^1}{V_{PCC}^0} \right) + p_P \right) \quad (13)$$

where, "0" and "1" denote for initial and next conditions. p_Z, p_I, and p_P are model coefficients limited to $p_Z + p_I + p_P = 1$ [32].

According to Table II, the evaluation has been carried out under various ZIP model coefficients. The data of these loads with unity power factor are taken from [32].

It is seen from the results in Fig. 10 that PCC voltage change would be more significant under the presence of ZIP load. In order to satisfy $P_L = P_{DG}$ in islanding mode, the PCC voltage is confronted with great variations whilst P_{DG} is declined by the disturbance. Hence, $ROCOV_2$ and $ROCOP_2$ cross the thresholds in such cases. Consecutive MPP lost is also evaded by deactivating the proposed algorithm after islanding detection.

E. Multiple-DGs Condition (Cases 28–31)

The connection of multiple GCPVSs at the same or nearby bus is practical to construct a PV power plant. From islanding detection standpoint, the connection of multi DGs may lead to interference of the applied disturbance and
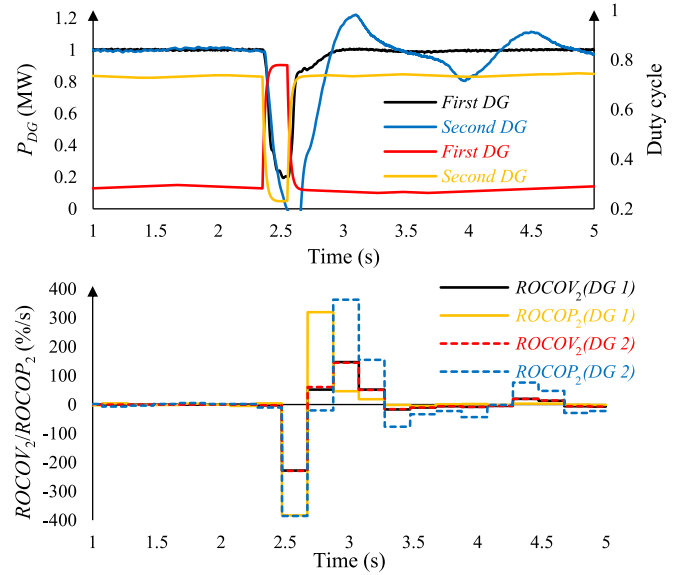

Fig. 11.   Results of multiple DGs scenarios in case 28.

misclassification [19]. The utility has been thereby disconnected at the presence of two GCPVSs in cases 28–31 under different power mismatches by opening CB$_1$ in Fig. 6.

Since the effect of active power reduction of all GCPVSs would be serious in non-islanding phenomena, the proposed methodology can be realized in two cases; all DGs equipped with the disturbance or a few DGs are responsible for islanding classification and sending the detection signal to remainder, called master-slave [19]. This study exploits the first scenario, i.e., both DGs are equipped with the suggested algorithm. The DGs' $ROCOV_2$ and $ROCOP_2$ of case 28 have been shown in Fig. 11. The outputs confirmed that the current IDM declines accurately these variables, irrespective of the converter topology, to surpass the stipulated margins for islanding detection purpose in at most 510 ms.

F. Non-Islanding Events (Case 32–44)

Despite effective islanding detection, the presented scheme should not exhibit nuisance tripping in non-islanding circumstances. Although the activation of the equipped disturbance in some non-islanding events is inevitable, high negative
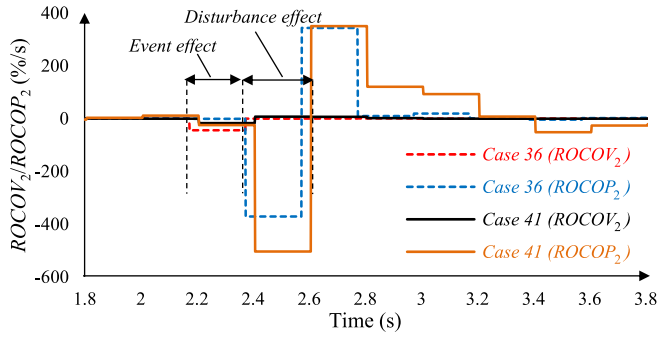
Fig. 12.   Outputs of capacitor disconnection and asynchronous motor starting.
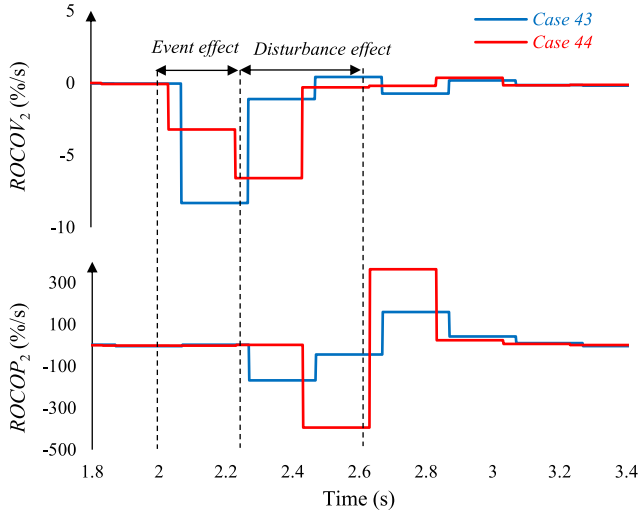

Fig. 13.   Results of the sudden load change.

values for $ROCOV_2$ and $ROCOP_2$ should not occur simultaneously. As detailed in Table III, several non-islanding switching events have been studied. This analysis focuses on scenarios with negative $ROCOV_2$, including capacitor bank disconnection, motor starting, and abrupt load raise (except case 44 with switching OFF the lead load). The results during the event and during disturbance activation are tabulated in Table III while DG output active power, voltage at the DG end, $ROCOV_2$, and $ROCOP_2$ of a few case studies are illustrated in Figs. 12 and 13.

It can be inferred that the PCC voltage variation is negligible ($ROCOV_1 < Th_1$) in cases 32, 37, and 38; hence, the proposed disturbance has not been stimulated. In other scenarios, the voltage drop results in a high negative $ROCOV_2$ as well as disturbance activation ($ROCOV_1 \geq Th_1$). The DG generation, however, remains unchanged for this time being and $ROCOP_2$ is near zero. When the disturbance is actuated, P_{DG} reduces markedly due to the MPP lost ($ROCOP_2 < Th_3$). Meanwhile, the PCC voltage has been re-established to its islanding steady-state level and $ROCOV_2$ is negligible. Therefore, the coincident high negative sets for $ROCOV_2$ and $ROCOP_2$ does not happen, indicating no false tripping of the proposed IDM in such disturbances.

V. COMPARISON WITH A FEW EXISTING ALGORITHMS

In literature, the NDZ, the detection time, the level of power quality degradation, the level of cost and complexity, and threshold determination are among the paramount reported features of IDMs. A comparison between several recent IDMs with the proposed strategy is carried out as follows and summarized in Table IV.

- First and foremost, the presented two-level scheme can detect islanding in all cases except for a narrow -0.4% to 0.4% range of $\Delta P/P_{DG}$, implying on its strong performance under a wide range of GCPVS operation.
- Computational-based IDMs are proven to be the fast and precise islanding classifiers; however, their settings highly depend on the case study system. Tedious tests should be thereby repeated for a different DG/system [12]–[18]. The disturbance gain of the active algorithms have also relied on the studied system characteristics [19]–[25]. Conversely, thresholds of the presented technique are determined by (4), (5) and (10)–(12), regardless of the DG and case study system settings.
- The recommended algorithm is designed so that it can be easily developed to multi-DGs case; however, the extension of equations in [25] is highly complex for multi-DGs scenario, especially for more than two units. The disturbance injection of multi DGs in [19] may also lead to the same outputs in the opposite direction; hence, islanding might be remained undetected from the overall outcome.
- In two-level IDMs, the total detection time includes data pre-processing time to identify suspicious islanding case, and the time to inject disturbance and observing its response, e.g., 1s for the presented algorithm in [28]. This time is at most 510 ms for the proposed technique, much lower the conventional IDMs and islanding standards.
- In a standalone microgrid, the backup systems are exploited to support critical loads and control frequency and voltage. The proposed technique is designed in a way that MPP is restored after islanding classification; the GCPVS can generate its maximum possible power in the autonomous microgrid to shorten the charging/discharging energy of the backup resources. Contrary to this, most active IDMs are structured to destabilize a local variable after island formation; thus, the DG output power is zero and maximum backup energy is needed [21]–[24].
- In the proposed two-level IDM, the PCC voltage and active power output are measured to quantify $ROCOV_1$, $ROCOV_2$, and $ROCOP_2$ and a disturbance is injected into the D_{MPP} under $ROCOV_1 \geq Th_1$ (Fig. 2). It can be thereby integrated into the existing VSIs by less than 200 USD, much lower than the hybrid and communication-based algorithms with 6,120 and 80,000 USD costs [6], [28].

VI. CONCLUSION

This article deals with a fast and accurate two-level algorithm for islanding detection of GCPVS. In the first level of the proposed IDM, a disturbance is triggered in the duty cycle

TABLE IV
COMPARISON OF SEVERAL RECENT IDMs WITH PROPOSED METHODOLOGY

Methodology	NDZ ($\Delta P/P_{DG}$)	Detection time range	Threshold dependency on system settings	Complexity of extension to multi-DGs	Power quality degradation?	Applicable to microgrid?	Cost and complexity
Commercial voltage relay [8]	-29 to 17%	Up to 2s	Low	Low	Low	Yes	Low
Rate of change of reactive power [9]	Near zero	Up to 100 ms	High	Low	No	Yes	Low
Rate of change of PCC resistance to angular velocity [10]	Near zero	Up to 201 ms	High	Low	No	Yes	Medium
Accumulate average of voltage [11]	Near zero	Up to 280 ms	Low	Low	No	Yes	Medium
PCC voltage's modal-based index [12]	Zero	Up to 66 ms	High	Low	Low	Yes	High
Autocorrelation of modal current [13]	Near zero	Up to 60 ms	High	Low	Low	No	High
Forced Helmholtz oscillator [14]	-12 to 10%	Up to 1.13s	High	Low	Low	Yes	High
Support vector machine [15]	Zero	Up to 60 ms	High	Low	No	Yes	High
Decision-tree [16]	Near zero	Up to 744 ms	High	Low	Low	Yes	Medium
Adaptive ensemble classifier [17]	Zero	Up to 120 ms	High	Low	Low	Yes	High
Deep learning [18]	Zero	Up to 150 ms	High	Low	Low	Yes	High
Impedance measurement [19]	Near zero	Up to 200 ms	High	High	High	Yes	High
Active slip frequency [20]	-2% to 2%	Up to 280 ms	High	Low	High	Yes	High
Active ROCOF relay [21]	Near zero	Up to 200 ms	High	Low	High	Yes	High
Voltage positive feedback (VPF) [22]	Up to 17%	Up to 500 ms	Medium	Low	Medium	No	Low
Improved VPF [23]	Near zero	Up to 300 ms	Medium	Low	High	No	Low
Voltage negative feedback [24]	Zero	Up to 900 ms	Medium	Low	Medium	No	Low
d–axis equivalent resistance [25]	Zero	Up to 800 ms	High	High	Medium	No	High
Parallel inductance switching [26]	Zero	Up to 300 ms	High	Low	Low	Yes	High
Reactive power disturbance with three passive IDMs [27]	Zero	Up to 173.7 ms	High	Low	Yes	No	High
Rate of change of reactive power and load connection [28]	Near zero	Up to 1s	High	Low	Low	Yes	High
Proposed algorithm	**Near zero**	**Up to 510 ms**	**Low**	**Low**	**Low**	**Yes**	**Low**

of the DC/DC converter when the measured ROCOV surpasses a threshold. This disturbance shifts GCPVS operating point from MPP, leading to simultaneous high negative values for ROCOV and ROCOP of the second level in islanding states. The proposed IDM has been examined under extensive real-time HiL simulation tests for a case study system with two large-scale PV systems. The outputs highlighted precise islanding classification within 510 ms irrespective of the power imbalance, load quality factor, and DG penetration even in multi DGs case.

According to the presented outcomes, the MPP has been restored after islanding detection through the MPPT algorithm. The GCPVS can thereby generate its maximum available power in microgrid after islanding classification unlike the conventional active IDMs. This feature is exploited as an opportunity for a fast reconnection and autonomous operation of GCPVS in microgrid structure.

Moreover, the comparative assessment of the proposed strategy with a few existing IDMs highlights its advancement in terms of simple and cost-effective implementation, and self-standing and straightforward threshold determination. Therefore, it can be simply integrated into the available VSIs as a strong and efficient tool for islanding detection purposes.

ACKNOWLEDGMENT

REFERENCES

[1] *Future of Solar Photovoltaic: Deployment, Investment, Technology, Grid Integration, and Socio-Economic Aspects*, Int. Renew. Energy Agency, Abu Dhabi, UAE, 2019.

[2] M.-S. Kim, R. Haider, G.-J. Cho, C.-H. Kim, C.-Y. Won, and J.-S. Chai, "Comprehensive review of islanding detection methods for distributed generation systems," *Energies*, vol. 12, no. 5, p. 837, Mar. 2019.

[3] *IEEE Standard for Interconnecting Distributed Resources With Electric Power Systems*, IEEE Standard 1547-2008, 2008.

[4] *Standard for Inverters, Converters, Controllers, and Interconnection System Equipment for Use With Distributed Energy Resources*, UL Standard 1741, Jan. 2010.

[5] V. Kleftakis, D. Lagos, C. Papadimitriou, and N. D. Hatziargyriou, "Seamless transition between interconnected and islanded operation of DC microgrids," *IEEE Trans. Smart Grid*, vol. 10, no. 1, pp. 248–256, Jan. 2019.

[6] B. Dob and C. Palmer, "Communications assisted islanding detection: Contrasting direct transfer trip and phase comparison methods," in *Proc. 71st Annu. Conf. Protective Relay Eng. (CPRE)*, Mar. 2018, pp. 1–6.

[7] G. Bayrak and E. Kabalci, "Implementation of a new remote islanding detection method for wind–solar hybrid power plants," *Renew. Sustain. Energy Rev.*, vol. 58, pp. 1–15, May 2016.

[8] J. C. M. Vieira, D. S. Correa, W. Freitas, and W. Xu, "Performance curves of voltage relays for islanding detection of distributed generators," *IEEE Trans. Power Syst.*, vol. 20, no. 3, pp. 1660–1662, Aug. 2005.

[9] S. Nikolovski, H. R. Baghaee, and D. Mlakic, "Islanding detection of synchronous generator-based DGs using rate of change of reactive power," *IEEE Syst. J.*, vol. 13, no. 4, pp. 4344–4354, Dec. 2019.

[10] R. Bekhradian, M. Davarpanah, and M. Sanaye-Pasand, "Novel approach for secure islanding detection in synchronous generator based microgrids," *IEEE Trans. Power Del.*, vol. 34, no. 2, pp. 457–466, Apr. 2019.

[11] A. G. Abd-Elkader, S. M. Saleh, and M. B. M. Eiteba, "A passive islanding detection strategy for multi-distributed generations," *Int. J. Elect. Power Energy Syst.*, vol. 99, pp. 146–155, Jul. 2018.

[12] Y. M. Makwana and B. R. Bhalja, "Experimental performance of an islanding detection scheme based on modal components," *IEEE Trans. Smart Grid*, vol. 10, no. 1, pp. 1025–1035, Jan. 2019.

[13] R. Haider *et al.*, "Passive islanding detection scheme based on autocorrelation function of modal current envelope for photovoltaic units," *IET Gener. Transm. Distrib.*, vol. 12, no. 16, p. 3911, Sep. 2018.

[14] M. Bakhshi, R. Noroozian, and G. B. Gharehpetian, "Novel islanding detection method for multiple DGs based on forced Helmholtz oscillator," *IEEE Trans. Smart Grid*, vol. 9, no. 6, pp. 6448–6460, Nov. 2018.

[15] H. R. Baghaee, D. Mlakić, S. Nikolovski, and T. Dragičević, "Anti-islanding protection of PV-based microgrids consisting of PHEVs using SVMs," *IEEE Trans. Smart Grid*, vol. 11, no. 1, pp. 483–500, Jan. 2020.

[16] Q. Cui, K. El-Arroudi, and G. Joós, "Islanding detection of hybrid distributed generation under reduced non-detection zone," *IEEE Trans. Smart Grid*, vol. 9, no. 5, pp. 5027–5037, Sep. 2018.

[17] A. Khamis, Y. Xu, Z. Y. Dong, and R. Zhang, "Faster detection of microgrid islanding events using an adaptive ensemble classifier," *IEEE Trans. Smart Grid*, vol. 9, no. 3, pp. 1889–1899, May 2018.

[18] X. Kong, X. Xu, Z. Yan, S. Chen, H. Yang, and D. Han, "Deep learning hybrid method for islanding detection in distributed generation," *Appl. Energy*, vol. 210, pp. 776–785, Jan. 2018.

[19] T. Bei, "Accurate active islanding detection method for grid-tied inverters in distributed generation," *IET Renew. Power Gener.*, vol. 11, no. 13, pp. 1633–1639, Nov. 2017.

[20] P. K. Ganivada and P. Jena, "An active slip frequency based islanding detection technique for grid-tied inverter," *IEEE Trans. Ind. Informat.*, vol. 16, no. 7, pp. 4615–4626, Jul. 2020.

[21] P. Gupta, R.S. Bhatia, and D.K. Jain, "Active ROCOF relay for islanding detection," *IEEE Trans. Power Del.*, vol. 32, no. 1, pp. 420–429, Feb. 2017.

[22] A. Samui and S. R. Samantaray, "An active islanding detection scheme for inverter-based DG with frequency dependent ZIP-exponential static load mode," *Int. J. Elect. Power Energy Syst.*, vol. 78, pp. 41–50, Jun. 2016.

[23] S. Liu, S. Zhuang, Q. Xu, and J. Xiao, "Improved voltage shift islanding detection method for multi-inverter grid-connected photovoltaic systems," *IET Gener. Transm. Distrib.*, vol. 10, no. 13, pp. 3163–3169, Oct. 2016.

[24] R. Bakhshi-Jafarabadi and J. Sadeh, "New voltage feedback-based islanding detection method for grid-connected photovoltaic systems of microgrid with zero non-detection zone," *IET Renew. Power Gener.*, vol. 14, no. 10, pp. 1710–1719, Jul. 2020.

[25] D. Sivadas and K. Vasudevan, "An active islanding detection strategy with zero non-detection zone for operation in single and multiple inverter mode using GPS synchronized pattern," *IEEE Trans. Ind. Electron.*, vol. 67, no. 7, pp. 5554–5564, Jul. 2020.

[26] A. Rostami, A. Jalilian, S. Zabihi, J. Olamaei, and E. Pouresmaeil, "Islanding detection of distributed generation based on parallel inductive impedance switching," *IEEE Syst. J.*, vol. 14, no. 1, pp. 813–823, Mar. 2020.

[27] X. Chen, Y. Li, and P. Crossley, "A novel hybrid islanding detection method for grid-connected microgrids with multiple inverter-based distributed generators based on adaptive reactive power disturbance and passive criteria," *IEEE Trans. Power Electron.*, vol. 34, no. 9, pp. 9342–9356, Sep. 2019.

[28] J. A. Laghari, H. Mokhlis, M. Karimi, A. H. A. Bakar, and H. Mohamad, "An islanding detection strategy for distribution network connected with hybrid DG resources," *Renew. Sustain. Energy Rev.*, vol. 45, pp. 662–676, May 2015.

[29] R. Dogga and M. K. Pathak, "Recent trends in solar PV inverter topologies," *Solar Energy*, vol. 183, pp. 57–73, May 2019.

[30] F. Belhachat and C. Larbes, "Comprehensive review on global maximum power point tracking techniques for PV systems subjected to partial shading conditions," *Solar Energy*, vol. 183, pp. 476–500, May 2019.

[31] *IEEE Recommended Practice for Utility Interface of Photovoltaic (PV) Systems*, IEEE Standard 929-2000, 2000

[32] M. W. Asres, A. A. Girmay, C. Camarda, and G. T. Tesfamariam, "Non-intrusive load composition estimation from aggregate ZIP load models using machine learning," *Int. J. Elect. Power Energy Syst.*, vol. 105, pp. 191–200, Feb. 2019.

Reza Bakhshi-Jafarabadi was born in Mashhad, Iran, in 1988. He received the M.Sc. and Ph.D. degrees in electrical engineering from the Ferdowsi University of Mashhad in 2014 and 2020, respectively.

In 2019, he was a visiting Ph.D. student with the Intelligent Electric Power Grids, TU Delft, The Netherlands. His research interests include renewable energy technologies, integration of distributed generators to the power system, and microgrid protection.

Javad Sadeh was born in Mashhad, Iran, in 1968. He received the B.Sc. and M.Sc. degrees (Hons.) in electrical engineering from the Ferdowsi University of Mashhad, Mashhad, in 1990 and 1994, respectively, and the Ph.D. degree in electrical engineering from the Sharif University of Technology, Tehran, Iran, with the collaboration of the Electrical Engineering Laboratory, Institut National Polytechnique de Grenoble, Grenoble, France, in 2001.

He is currently a Professor with the Department of Electrical Engineering, Ferdowsi University of Mashhad, where he is also an Educational Office Manager. His research interests are power system protection, dynamics, operation as well as renewable energy technologies.

Jose de Jesus Chavez (Member, IEEE) received the M.Sc. and Ph.D. degrees from the Center for Research and Advanced Studies, National Polytechnic Institute, Mexico City, in 2006 and 2009, respectively. In 2009, he was a visiting Ph.D. student with the RTX-LAB, University of Alberta, Canada. He joined the Technological Institute of Morelia, Mexico, as an Assistant Professor in 2010, where he was a Full Professor in 2012, and the Chair of the Graduate and Research Program in electrical engineering from 2014 to 2016. He was a Postdoctoral Member with TU Delft, The Netherlands, from 2016 to 2020. He is currently a Professor with the National Technological Institute of Mexico. His research interests include electromagnetic transients, harmonics analysis, digital protective relays, and real-time simulation.

Marjan Popov (Senior Member, IEEE) received the Dipl.-Ing. degree in electrical power engineering from the University of Saints Cyril and Methodius, Skopje, North Macedonia, in 1993, and the Ph.D. degree in electrical power engineering from the Delft University of Technology, Delft, The Netherlands, in 2002.

He is also a Chevening Alumnus and was an Academic Visitor with the University of Liverpool, Liverpool, U.K., working in the Arc Research Group on modeling SF6 circuit breakers, in 1997. His major fields of interest are in future power systems, large-scale power system transients, intelligent protection for future power systems, and wide-area monitoring and protection. He is a Member of CIGRE and actively participated in WG C4.502 and WG A2/C4.39. He received the prestigious Dutch Hidde Nijland Prize for extraordinary research achievements in 2010. He is an IEEE PES Prize Paper Award and an IEEE Switchgear Committee Award recipient in 2011 and an Associate Editor of the *International Journal of Electric Power and Energy Systems* (Elsevier).